Surfactant-based interface capture towards the development of 2D-printed photonic structures

Appurva Tiwari[1], Seong Jae Lee[2], Ashish Kumar Thokchom[1]*

[1]Soft Matter Lab, Department of Chemical Engineering, Shiv Nadar Institution of Eminence Deemed to be University, Greater Noida, India – 201314

[2]Department of Polymer Engineering, The University of Suwon, Hwaseong, Gyeonggi, South Korea – 18323

***Corresponding Author:**

Ashish Kumar Thokchom, Ph.D.

Soft Matter Lab, Department of Chemical Engineering, Shiv Nadar Institution of Eminence Deemed to be University, Greater Noida, India – 201314

Email: ashish.thokchom@snu.edu.in

Ph: +91 361 2582259

1. Profilometry of the deposition structure

To provide further insight into the morphology of the deposition structure obtained in the presence and absence of cetyltrimethylammonium bromide (CTAB), the corresponding depositions are analyzed using surface profilometry. As shown in Fig. S1a, the droplet without CTAB forms a ring-like deposition profile with random particle distribution inside the ring. This is further confirmed by the deposition height versus distance along an arbitrary cross-section along the droplet center in Fig. S1b. Contrarily, the deposition profile of the droplet containing CTAB shows significantly suppressed ring formation and a monolayer deposition of the particle inside the ring Fig. S1(c and d).

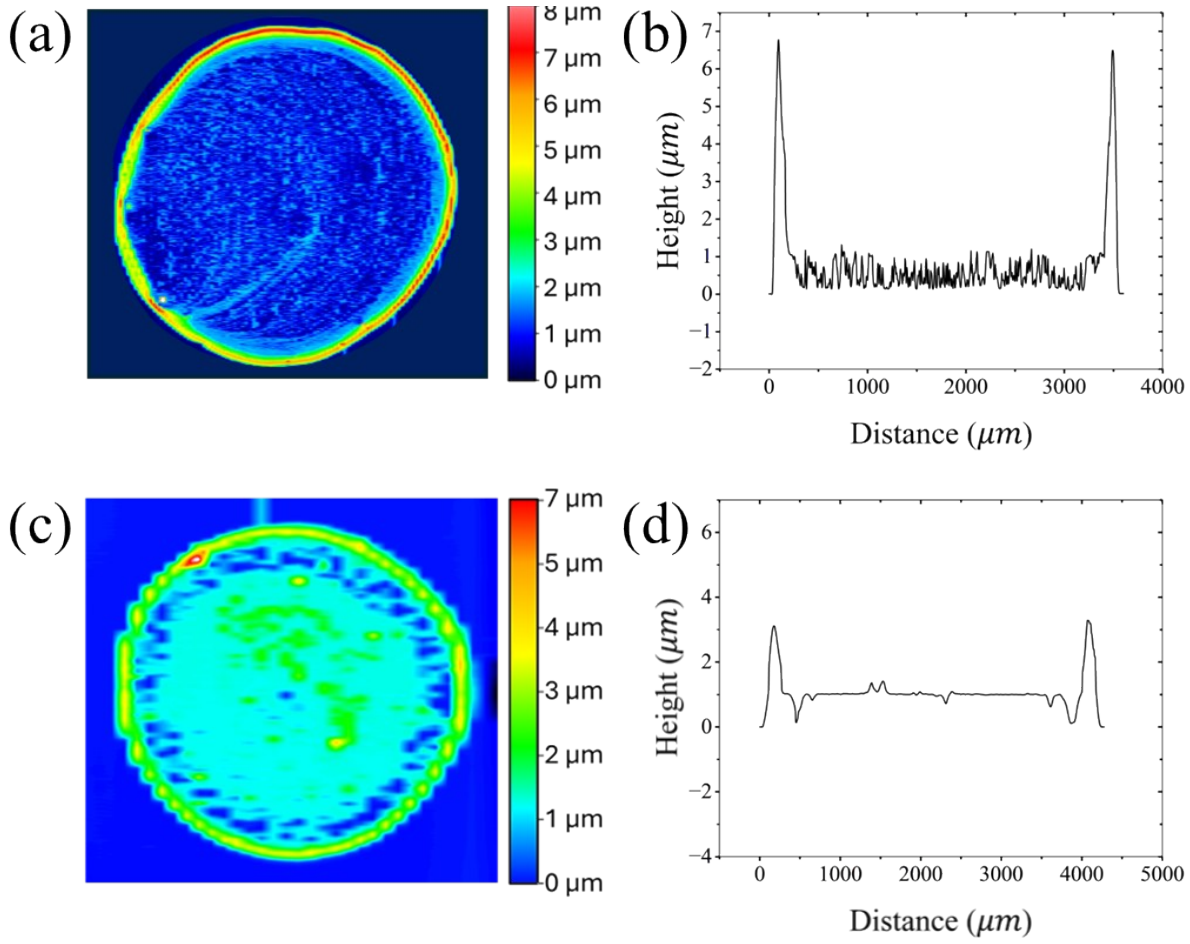

Fig. S1. The surface profilometer analysis of the deposition structure obtained (a,b) without and (c,d) with CTAB (0.05 wt%) at 1.5 wt% polystyrene (PS) particle concentration and droplet volume of 1.5 µl.

2. The monolayer deposition of CTAB-laden droplet

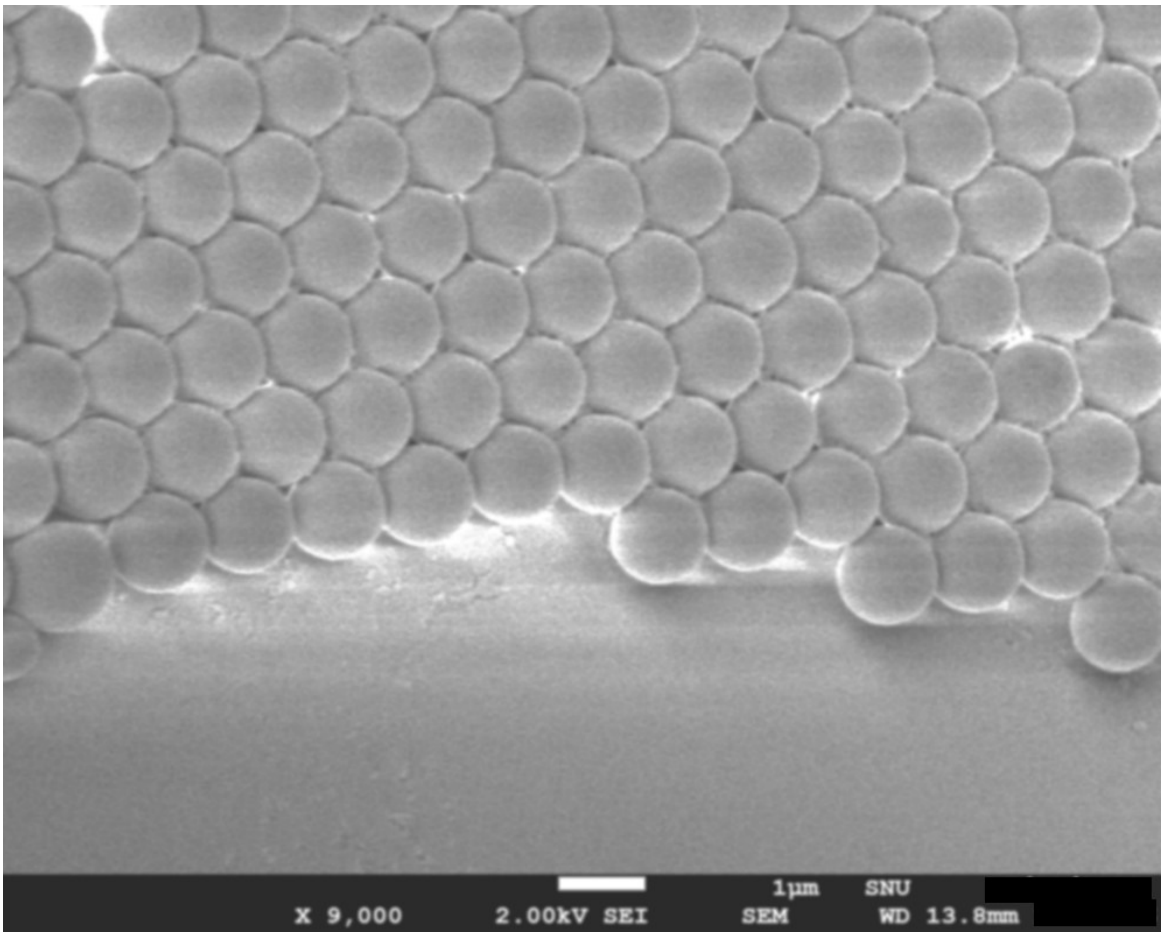

Fig. S2. The SEM image showing the perspective view of monolayer particle arrangement in the deposition formed by the droplet containing 1.5 wt% PS particle and 0.05 wt% CTAB.

3. The formation of particle aggregates at the gas-liquid (G-L) interface

During the evaporation of a surfactant-laden colloidal droplet containing 0.05 wt% CTAB and 1.5 wt% PS particles, the particles are observed to be captured at the G-L interface. The capturing of the particles is attributed to the hydrophobization of the particle surface due to the adsorption of the CTAB on the particle interface.[1-3] As the droplet evaporates, the captured adjacent particles begin to interact due to lateral capillary meniscus forces.[4] These capillary forces draw the particles closer together, leading to the gradual formation of small, well-

ordered PS aggregates, as depicted in Fig. S3. Over time, these aggregates merge together to form an interfacial film, as shown in Video S1.

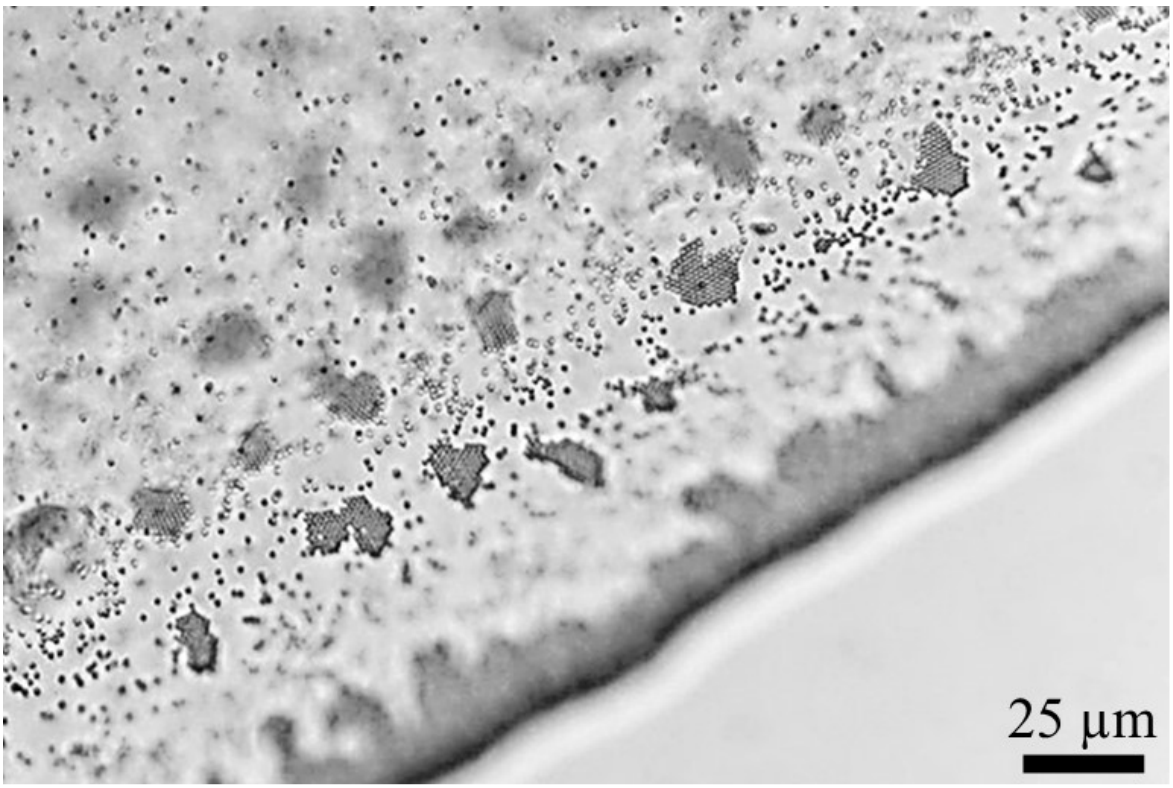

Fig. S3. The small ordered 2-D particle aggregates formed at the interface of the evaporating droplet at 0.05 wt% dissolved CTAB and 1.5 wt% dispersed PS particle concentrations.

4. Influence of surfactant on particle wettability

To determine the effect of CTAB on PS particle hydrophobicity, the contact angle of water droplets on films of PS particles with and without CTAB is measured. Films are prepared by depositing PS suspensions onto glass slides after removing excess liquid. The contact angle of a water droplet on each film is measured six times, and the mean value is calculated. As shown in Fig. S4, the contact angle on the bare PS film is approximately $68.16° \pm 1.94°$. Addition of 0.05 wt% CTAB significantly increases the contact angle to $104° \pm 2°$, indicating enhanced hydrophobicity. This is ascribed to CTAB adsorption, where positively charged CTAB electrostatically interacts with negatively charged PS particles, presenting hydrophobic tails to

the surface. However, at 0.15 wt% CTAB, the contact angle decreases to $40.33° \pm 2.16°$, suggesting reduced hydrophobicity. This can be attributed to the formation of a second CTAB layer driven by hydrophobic interactions between CTAB tails, effectively shielding the initially exposed hydrophobic surface. The observed trend in contact angle with increasing CTAB concentration aligns with previous studies on surfactant-particle interactions.[3]

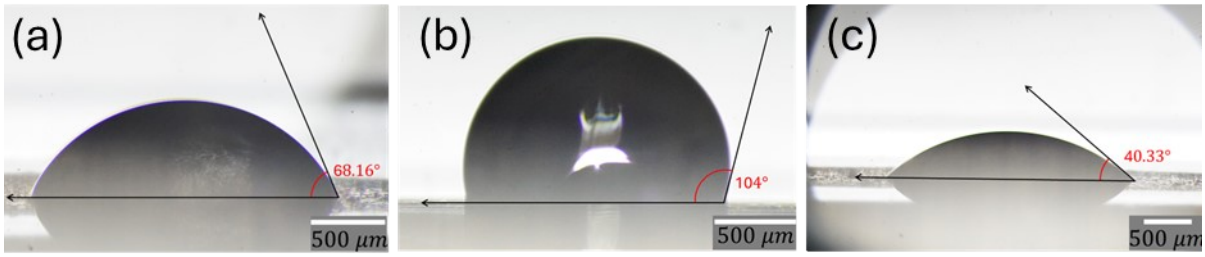

Fig. S4. The contact angle of a water droplet on the film of (a) only PS suspension, (b) PS suspension containing 0.05 wt% CTAB, and (c) PS suspension containing 0.15 wt% CTAB.

5. Influence of surfactant on particle adsorption energy, E

The measured contact angle values corresponding to the surfactant concentration are further used to calculate the particle adsorption energy at the G-L interface, $E = \pi R^2 \gamma_{LG}(1 - \cos\theta)^2$.[5] Where, R ($1\ \mu m$) is the radius of the microparticle and γ_{LG} (34 mN/m with 0.05 wt% CTAB and 72mN/m without CTAB) is the liquid-air surface tension. The difference in the calculated values of particle adsorption energy with (0.05 wt%) and without CTAB, $\Delta E = E_{0.05\,wt\%} - E_{0\,wt\%}$ is found to be 4.63 x 10^6 kT. This suggests a significant improvement in the tendency of the particle to remain captured at the G-L interface. However, ΔE was found to be -5.01 x 10^6 kT at 0.15 wt% CTAB, demonstrating a considerable decrease in E at higher CTAB concentration.

6. Influence of surfactant on interparticle capillary meniscus force

Subsequently, the influence of CTAB-induced particle hydrophobicity on the capillary meniscus force between the particles at the interface is estimated using the following expression:[4]

$$F_{cmf} = 2\pi\gamma_{LG}RBo^{\frac{5}{2}}S^2K_1(dq)$$

Where $Bo = qR^2$ is the Bond number, d is the interparticle distance, q = $\sqrt{(\rho_{liq} - \rho_{air})g/\gamma_{LG}}$ is the inverse of capillary length, $S = \frac{2}{3}D - \frac{1}{3} - \frac{1}{2}cos\theta + \frac{1}{6}cos^2\theta$ and K_1 is the first-order modified Bessel function of the second kind. D is calculated as, $D = \frac{\rho_{PS} - \rho_{air}}{\rho_{liq} - \rho_{air}}$. The values are calculated using θ corresponding to the CTAB concentration shown in Fig. S4, $\rho_{liq} = 995.65\ kg/m^3$, $\rho_{air} = 1.1644\frac{kg}{m^3}$, $\rho_{PS} = 1050\ kg/m^3$, $\gamma_{LG} = 34\ mN/m$ with CTAB and 72 mN/m without CTAB). The calculated values at varying non-dimensional (d/R) interparticle distances are shown in Fig. S5. The values at 0.05 wt% CTAB are found to be 6.3 times higher than without CTAB. Notably, the capillary meniscus force between the particles is significantly decreased at 0.15 wt% CTAB.

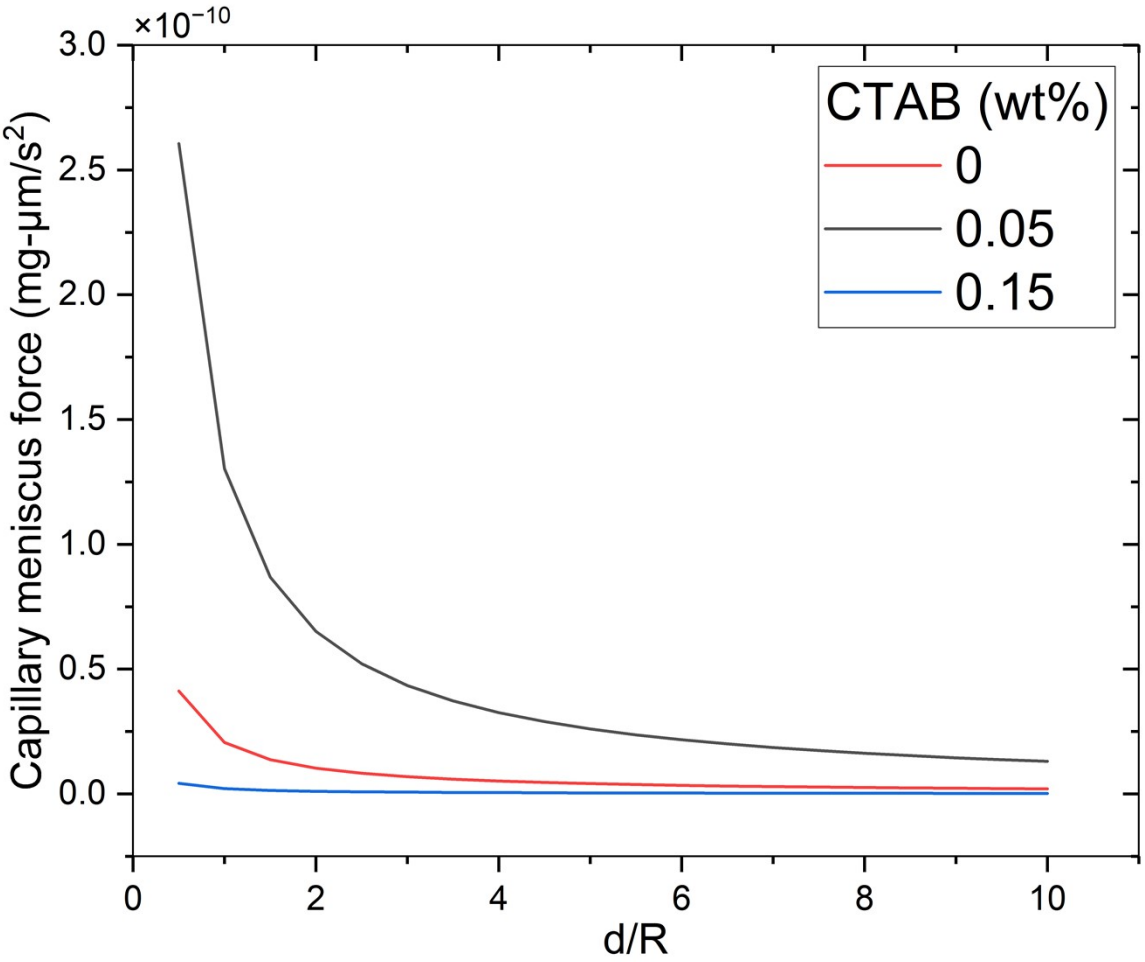

Fig. S5. The dependence of capillary meniscus force between the particles captured at the G-L interface at different CTAB concentrations. The difference is attributed to the change in the particle wettability with CTAB concentration shown in Fig. S4.

7. Confocal laser scanning microscopy-based analysis of CTAB distribution

This section reports an experimental analysis of CTAB concentration distribution within an evaporating sessile droplet to supplement the mechanism of the surfactant-induced Marangoni flow generation discussed in the main manuscript. The concentration profile of fluorescein-labeled CTAB (0.025 wt%) inside the droplet is determined through fluorescence intensity measurements using confocal laser scanning microscopy (Nikon Ti2E, A1R MP), with excitation and emission wavelengths of 488 nm and 530 nm, respectively. The variation in the intensity along the droplet radius is analyzed using ImageJ, at different time intervals (Fig. S6).

The lateral profile of the droplet is captured using a digital camera (Sony ZV-E10) equipped with a microscope lens (Kron Technologies), positioned laterally to the droplet. The initial intensity profile is normalized to the droplet height profile and calibrated using known initial CTAB concentration. This calibration allowed the conversion of intensity data into concentration profiles, as shown in Fig. S7. The detailed procedure of the analysis is provided in a study by Kajiya et al. 2008.[6]

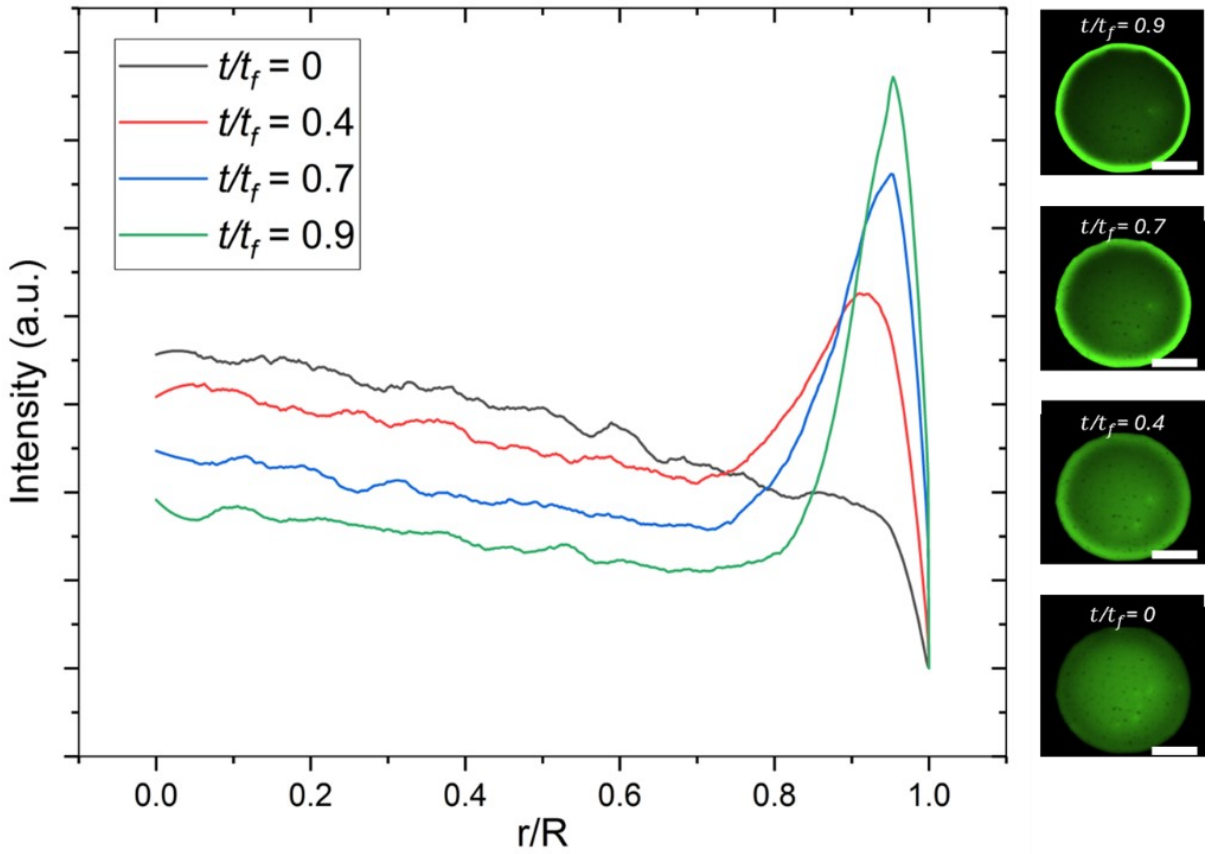

Fig. S6. The intensity values at varying normalized droplet radius (r/R) for different time intervals.

The surface tension values for different CTAB concentrations are adapted from existing literature[7] and replotted, as shown in Fig. S8a. A curve-fitting equation is obtained from the plotted values. The surface tension values for varying CTAB concentrations along (R-r/R) are further calculated using the equation, which are graphically represented in Fig. S8b.

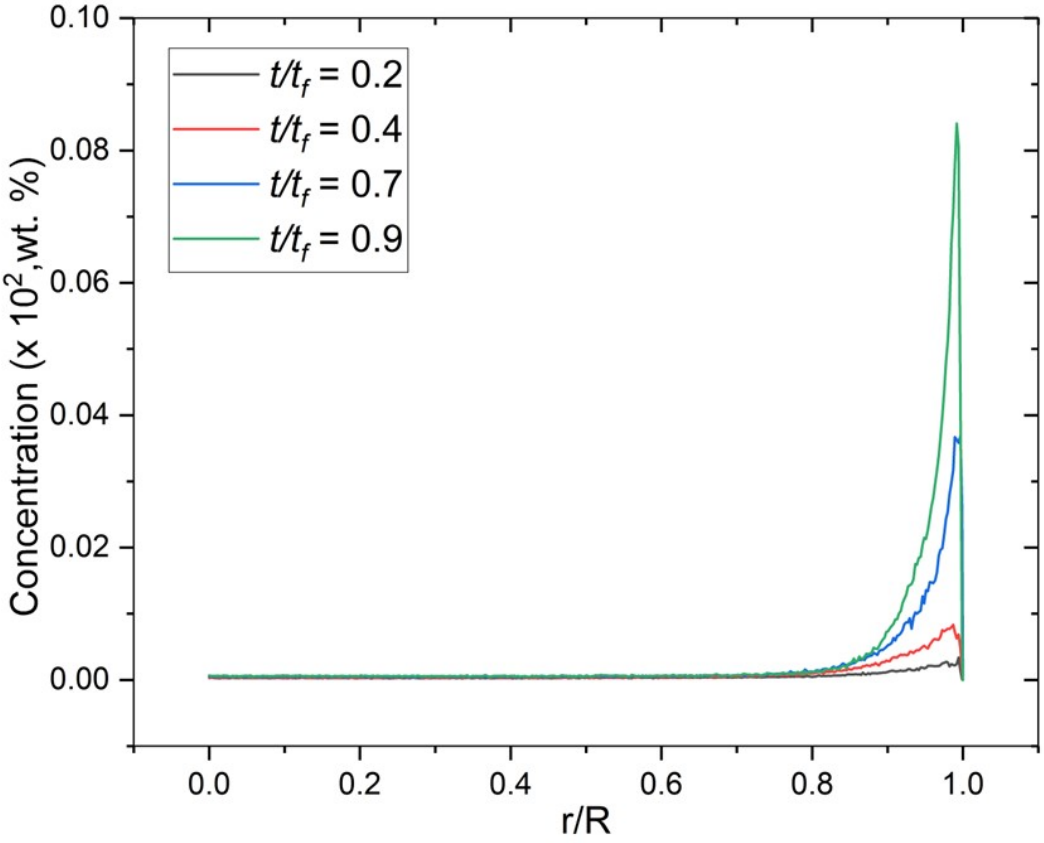

Fig. S7. The CTAB concentration value at varying normalized droplet radius (r/R) at different time intervals.

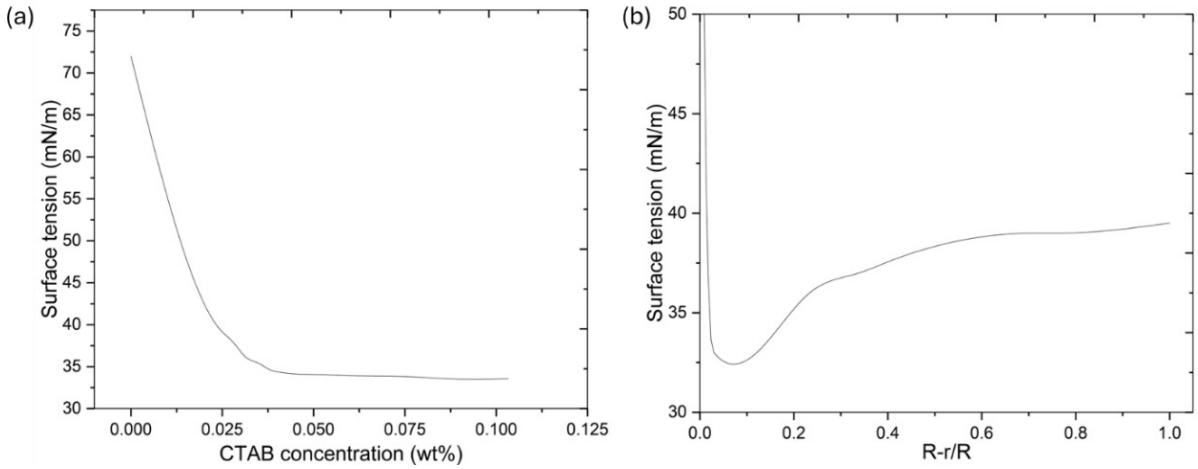

Fig. S8. Analysis of the surface tension variation inside an evaporating CTAB containing sessile droplet. (a) Surface tension as a function of CTAB concentration[7] and (b) the calculated surface tension values (using a curve fitting equation obtained from Fig. 8a) along the normalized radius (R-r/R) at t/t_f =0.1.

8. The Iridescent characteristic of surfactant-based deposition

The iridescent nature of the ordered monolayer particle deposition of the CTAB-laden colloidal droplet is characterized using the method shown in Fig. S9. The method is adopted from existing literature and allows simple observation of angle dependence of the deposition structural color via a single image.[8,9] In this technique, the sample deposition is illuminated with collimated white light oriented perpendicular to the sample surface, and the reflection is captured within a hemispherical dome, as depicted in Fig. S9a. The droplet deposition illustrated in Fig. 1d of the main manuscript is utilized as the sample. The projected colors are mapped linearly according to the polar angle (α) and azimuthal angle (∅). The red, green, and blue (RGB) intensities, averaged over ∅, are measured against α using the ImageJ software,[10] as presented in Fig. S9b. Moreover, the angle dependence of the structural color reveals the diffraction grating-like behavior of the deposition.[8,11] Hence, as a further analysis, the theoretical particle diameter is calculated using the grating equation:

$$m\lambda = d(sin\alpha_i + sin\alpha_r)$$

where d is the grating spacing calculated as $d = \frac{\sqrt{3}}{2}D$ for hexagonal particle arrangement. D is the interparticle center-to-center distance, 'm' is the diffraction order, α_i and α_r are the angles formed by the incident and diffracted rays relative to the normal of the deposition sample. Since the sample is illuminated normally, the value of α_i=0. Using m=1, α_r values corresponding to peak intensity (Fig. S9b) and peak wavelengths (λ) of 460 nm, 545 nm, and 680 nm for the blue, green, and red channels, respectively, the estimated particle diameter is determined to be approximately 1 μm.[8] This estimation is in excellent agreement with the actual particle diameter used in the study, validating the accuracy of the method and the consistency of the experimental results.

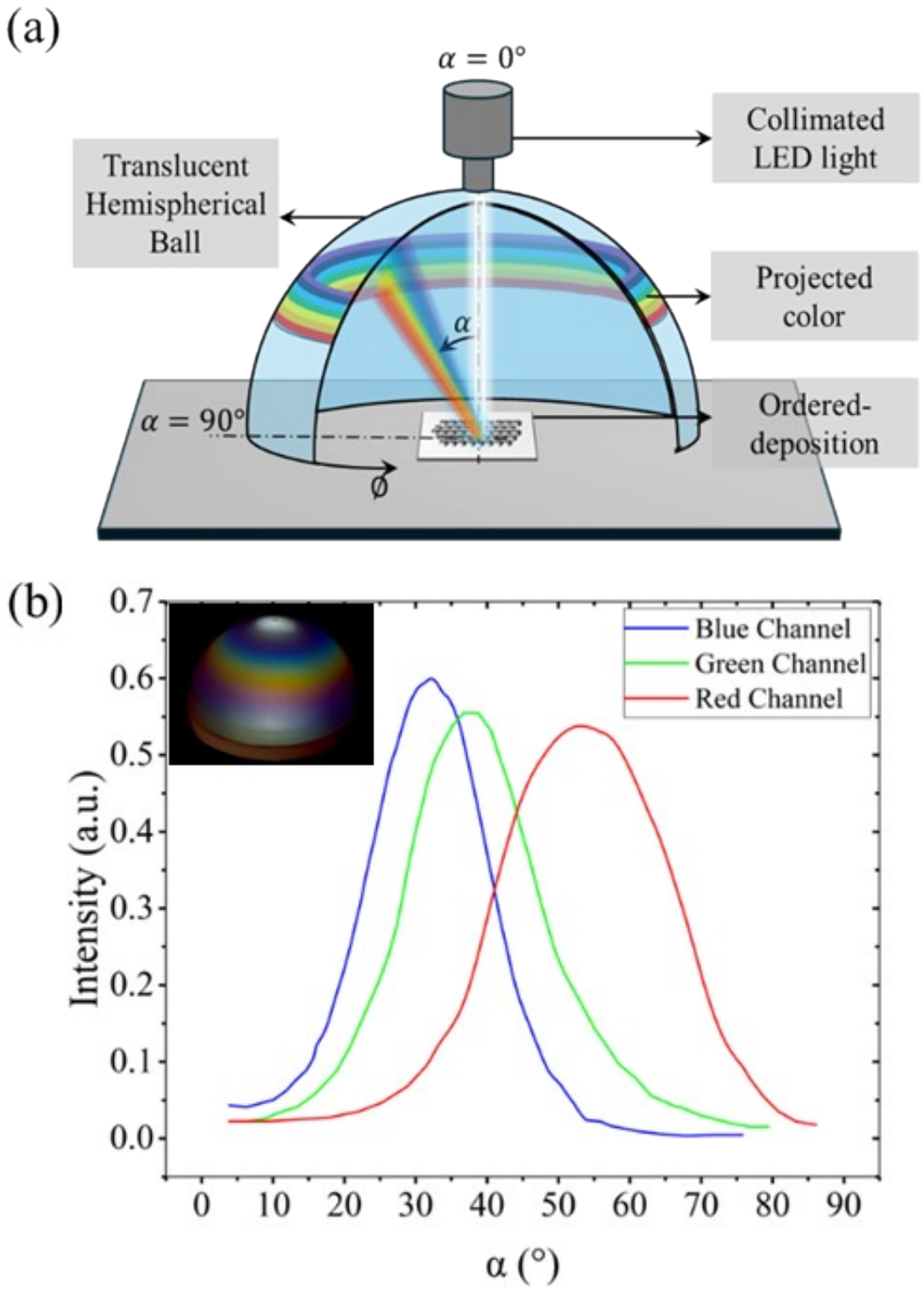

Fig. S9. The iridescent characteristics of the surfactant-based ordered monolayer deposition. (a) A schematic representation of the method adopted to observe the angle-dependent structural color separation on a hemispherical dome. (b) The graph shows the intensity variation with α for RGB channels. The inset image shows the digital photograph of the captured angle-based separation of structural color observed on the hemispherical dome.

9. Interfacial film formation at different surfactant concentrations

The formation of the interfacial film significantly depends on the dissolved CTAB concentrations. Fig. S10 shows the top-view image of the evaporating colloidal droplet containing 1.5 wt% PS particles and different CTAB concentrations. The images are captured at t* = 0.9, where t* is the ratio of the evaporation time at which the image is captured to the total evaporation time. Evidently, no film formation is observed at 0.0015 wt%, while the particles are captured at the interface at CTAB concentrations of 0.0075 wt% and 0.05 wt%. A further increase in the CTAB suppresses the film formation. This difference in the tendency of particles being captured at the interface forming a film significantly depended on particle hydrophobicity determined by the extent of CTAB absorption on the particle surface. At the same time, the extent of CTAB adsorption on the particle surface depends on the concentration of CTAB in the colloidal solution, as confirmed by the zeta potential measurements in Fig. 4f. Moreover, the difference in the region of the film formation at CTAB concentrations of 0.0075 wt% and 0.05 wt% is ascribed to the alteration in the internal flow at higher CTAB concentrations. The details are discussed in the main manuscript.

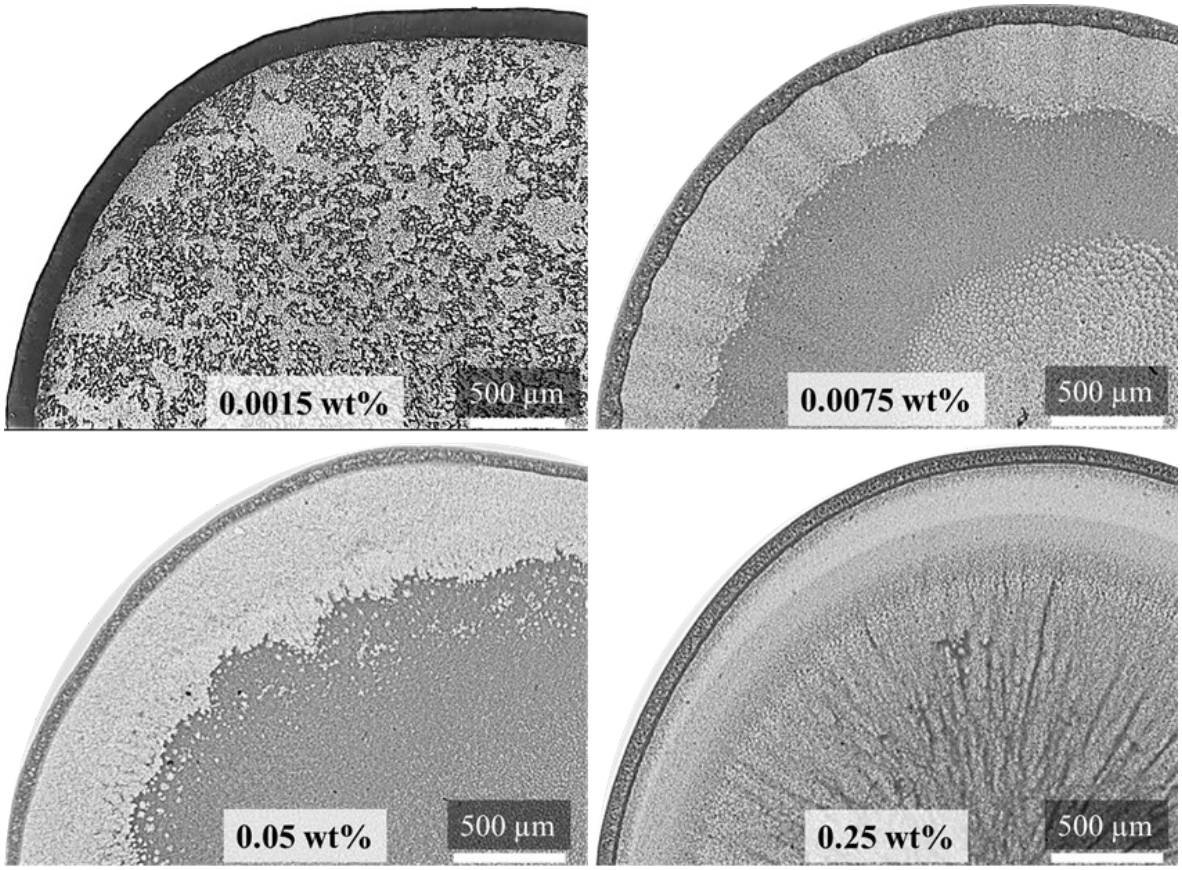

Fig. S10. Dependence of particle film formation on CTAB concentration. The captured images of evaporating droplets containing 1.5 wt% PS particles and varying dissolved CTAB concentrations at $t^* = 0.9$.

10. The adsorption of CTAB on the PS microsphere

The adsorption behavior of CTAB on the surface of PS microspheres can be described by the Somasundaran-Fuerstenau isotherm (four region adsorption theory), the most common isotherm for oppositely charged surfactant-surface systems.[12] This isotherm is divided into four distinct regions, as illustrated in Fig. S11a. In region I, the diffusion of the surfactant molecules from the bulk liquid towards the oppositely charged surface occurs and adsorption is primarily caused by the electrostatic attraction between the charged surface and the surfactant head groups (Fig. S11b). The surfactants remain sparsely distributed as individual hemimicelle without interacting with one another. The adsorption density is low. In region II, the surfactant adsorption on the surface i.e., hemimicelle formation continues, primarily due to surfactant-surface electrostatic interaction, reducing the surface charge. However, the adsorption can also be contributed by hydrophobic interaction between the hemimicelle and the surfactant molecules (Figure S11c) resulting in the simultaneous formation of admicelles, causing increased surfactant adsorption. In region III, the surface is neutralized, i.e., saturated with hemi micelles, and further adsorption is mainly driven by hydrophobic interactions. Thus, the rate of surfactant adsorption is decreased. Region IV represents a plateau where the adsorption density stabilizes. The surface becomes fully saturated, and additional surfactant molecules form micelles or aggregates in the bulk solution.

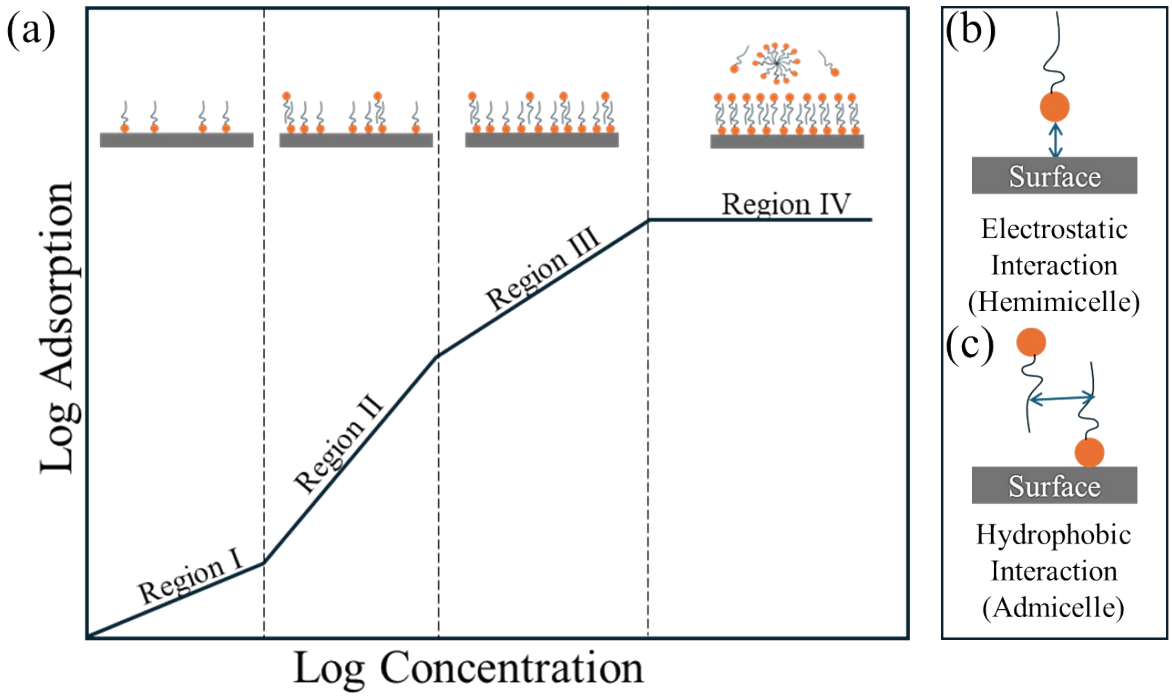

Fig. S11. (a) The Somasundaran−Fuerstenau isotherm for adsorption of ionic surfactant on oppositely charged surfaces.[12] (b) The surfactant-substrate electrostatic and (b) surfactant-surfactant hydrophobic interactions.

11. Flexible photonic structures

As discussed in the main manuscript, the printed monolayer structure is replicated on a PDMS using a soft lithography technique. Interestingly, apart from being flexible, the replicated structure is covert and becomes visible manifesting structural colors at certain viewing conditions, as demonstrated in Fig. S12.

Fig. S12. The flexible photonic structure fabricated by replicating printed monolayer photonic structure (shown in inset Fig. 6c of the main manuscript) on PDMS using soft lithography.

12. Supporting Videos

Video S1. The video shows a top view of a sessile droplet containing 0.05 wt% CTAB and 1.5 wt% PS particles. As the droplet evaporates, the particles progressively cluster at the G-L interface, forming an interfacial film. The particle arrangement in this film is subsequently observed, revealing the formation of a highly ordered, closely packed monolayer structure. This film deposits to form an ordered monolayer particle arrangement, which manifests structural colors, as further illustrated in Video S4.

Video S2. The video shows confocal laser microscopy observations of variations in the distribution of CTAB within an evaporating sessile droplet. With progress in time the surfactant accumulates near the droplet contact line while the droplet central region is depleted. This is attributed to non-uniform evaporation-driven radial outward flow. The observation supports the existence of a CTAB concentration gradient between the contact line and droplet apex. Such a gradient results in a surface tension difference, generating a radially inward Marangoni flow from the region of lower surface tension (contact line) to the region of higher surface tension (apex). The capture Marangoni flow of the particles is shown in Video S3.

Video S3. The video visualizes the Marangoni flow observed near the contact line of the evaporating colloidal droplet containing 0.05 wt% CTAB. This flow arises from a non-uniform CTAB concentration distribution between the contact line and droplet center as confirmed in Video S2. The video clearly illustrates the interfacial transport of individual particles and small aggregates, originating at the contact line and extending radially inwards towards the droplet center due to Marangoni flow. This facilitates their efficient distribution across the droplet interface and plays a crucial role in propelling individual particles or smaller aggregates towards larger “islands” trapped at the interface, ultimately contributing to the formation of a monolayer film.

Video S4. The video demonstrates the structural color of the deposition structure formed by the evaporation of a colloidal droplet containing 0.05 wt% CTAB. The deposition is illuminated using a collimated white light source which is fixed perpendicularly (normal) to the surface of the deposition. The structural color is recorded using a smartphone (iPhone). Evidently, the structural colors of the deposition layer change depending on the viewing angle i.e., the deposition shows iridescence. This is attributed to a diffraction grating-like behavior of the deposition, as discussed in the main manuscript.

Video S5. The video showcases the drop-by-drop printing method of the colloidal solution containing 0.05 wt% CTAB and 1.5 wt% PS particles. This method involves dispensing the solution at a controlled rate of 2.50 μL/min, producing an array of nanoliter droplets (~21 nL each). These droplets are delivered at a frequency of approximately two per second. The droplets deposit to form an ordered monolayer similar to the single droplet observations reported in the study. Hence the printed array manifests structural colors, as illustrated in the accompanying inset image. The findings demonstrate that the proposed interface capture method of photonic crystal formation and the printing technique can be simultaneously applied to the fabrication of large-scale photonic materials.

Video S6, The video demonstrates the particle capture at the interface during the direct writing of the same colloidal solution used for drop-by-drop printing, a phenomenon analogous to that observed in single-droplet experiments. This underscores the potential of the interface capture method to be applied to direct writing of the colloidal crystals, allowing the fabrication of customized photonic patterns as shown in Fig. 6c of the main manuscript.

Video S7. The video illustrates the formation of a monolayer particle deposition using the direct writing technique. The colloidal solution with 1.5 wt% PS particles and 0.05 wt% CTAB wt% is directly written onto a glass substrate at a speed and dispense rate of 5500 μm/s and 25

μl/s, respectively. The resulting highly ordered and closely packed monolayer arrangement of particles, is depicted in Fig. 6c. The customized pattern produced through this technique displays vibrant structural colors.

Video S8. The video demonstrates the formation of a sub-monolayer particle deposition achieved through the direct writing of colloidal solution at a lower PS particle concentration of 0.75 wt% and higher printing speed of 6500 μm/s compared to that used to form monolayer deposition. However, the CTAB concentration (0.05 wt%) and dispense rate (25 μl/min) are kept fixed. The resultant deposition remains ordered but with voids within the structure. These voids contribute to the overall higher transparency of the deposited material, allowing it to achieve a covert appearance while maintaining its structural integrity. Notably, despite the transparency, the deposited structure retains its ability to produce structural color when exposed to white light or daylight, as shown in Video S9. This further shows the potential interface capture-based fabrication of structures for applications requiring transparency, such as anti-counterfeiting by simple interplay between deposition speed and particle concentration.

Video S9, The video highlights the covert-overt feature of patterns with sub-monolayer deposition under both, day and white light illumination. While the printed patterns appear transparent and unobtrusive under normal viewing conditions, they display vivid structural colors when observed from specific angles. This phenomenon demonstrates that the photonic properties of the particles are preserved even at sub-monolayer coverage.

References

1. K. N. Al-Milaji and H. Zhao, *The Journal of Physical Chemistry C*, 2019, **123**, 12029-12041.

2. M. Anyfantakis and D. Baigl, *Chemphyschem*, 2015, **16**, 2726-2734.

3. S. Zhang, Q. Lan, Q. Liu, J. Xu and D. Sun, *Colloids and Surfaces A: Physicochemical and Engineering Aspects*, 2008, **317**, 406-413.

4. X. Ma, N. N. Nguyen and A. V. Nguyen, *Adv Colloid Interface Sci*, 2022, **307**, 102731.

5. M. Anyfantakis, Z. Geng, M. Morel, S. Rudiuk and D. Baigl, *Langmuir*, 2015, **31**, 4113-4120.

6. T. Kajiya, D. Kaneko and M. Doi, *Langmuir*, 2008, **24**, 12369-12374.

7. S. K. Shah and A. Bhattarai, *Journal of Chemistry*, 2020, **2020**, 1-13.

8. A. T. L. Tan, S. Nagelberg, E. Chang-Davidson, J. Tan, J. K. W. Yang, M. Kolle and A. J. Hart, *Small*, 2020, **16**, e1905519.

9. A. Tiwari, S. J. Lee, D. K. Garg, S. Shin and A. K. Thokchom, *Langmuir*, 2024, **40**, 8711-8720.

10. C. A. Schneider, W. S. Rasband and K. W. Eliceiri, *Nature Methods*, 2012, **9**, 671-675.

11. C. Park, K. Koh and U. Jeong, *Scientific Reports*, 2015, **5**, 8340.

12. S. Kalam, S. A. Abu-Khamsin, M. S. Kamal and S. Patil, *ACS Omega*, 2021, **6**, 32342-32348.